JSHC
Japan Society of
Histochemistry and Cytochemistry
Established 1959

Acta Histochem. Cytochem. 51 (5): 153–165, 2018
doi: 10.1267/ahc.18018

Immunocytochemical Localization of Choline Acetyltransferase in the Microbat Visual Cortex

Gil-Hyun Kim, Hang-Gu Kim and Chang-Jin Jeon

Department of Biology, School of Life Sciences, BK21 Plus KNU Creative BioResearch Group, College of Natural Sciences, and Brain Science and Engineering Institute, Kyungpook National University, Daegu 41566, South Korea

Received April 27, 2018; accepted August 17, 2018; published online September 29, 2018

The purpose of the present study was to investigate the organization of choline acetyltransferase (ChAT)-immunoreactive (IR) fibers in the visual cortex of the microbat, using standard immunocytochemistry and confocal microscopy. ChAT-IR fibers were distributed throughout all layers of the visual cortex, with the highest density in layer III and the lowest density in layer I. However, no ChAT-IR cells were found in the microbat visual cortex. ChAT-IR fibers were classified into two types: small and large varicose fibers. Previously identified sources of cholinergic fibers in the mammalian visual cortex, the nucleus of the diagonal band, the substantia innominata, and the nucleus basalis magnocellularis, all contained strongly labeled ChAT-IR cells in the microbat. The average diameter of ChAT-IR cells in the nucleus of the diagonal band, the substantia innominata, and the nucleus basalis magnocellularis was 16.12 μm, 13.37 μm, and 13.90 μm, respectively. Our double-labeling study with ChAT and gamma-aminobutyric acid (GABA), and triple labeling with ChAT, GABA, and post synaptic density 95 (PSD-95), suggest that some ChAT-IR fibers make contact with GABAergic cells in the microbat visual cortex. Our results should provide a better understanding of the nocturnal bat visual system.

Key words: visual cortex, choline acetyltransferase, microbat, immunocytochemistry

I. Introduction

Bats are widely distributed around the world and are the second most common mammalian species after rodents. Bats are nocturnal mammals that have the capacity for flight [1, 18, 58, 65]. In general, bats are known to have degenerated eyes and to search for food or hunt primarily by using sophisticated laryngeal echolocation, that is, they acoustically perceive their environment by interpreting returning echoes of emitted sounds [12, 32, 39, 53, 57, 67, 68, 70]. Bats are generally divided into two suborders: *Megachiroptera* (Megabats, approximately 200 species, 40–220 cm wingspan), also known as fruit bats, which have large eyes and use vision to track wings and food, and *Microchiroptera* (Microbats, approximately 800 species, 22–135 cm wingspan), which are known to have small eyeballs and somewhat decreased visual acuity. It was discovered, however, that many microbats also depend on visual information for perception, predatism, and self-defense [3, 27, 69, 72, 75, 76]. Several studies have demonstrated the existence of photoreceptors, rod and cone bipolar cells, and subtypes of amacrine and retinal ganglion cells, in microbats [10, 17, 36, 37, 42, 54, 55, 59, 62], suggesting that the microbat might have functional organization for its visual system. The microbat visual cortex has also been used to study the cytoarchitecture of calcium-binding protein-containing neuronal populations [22, 41], and nitric oxide synthase-containing neurons [26].

Acetylcholine (ACh), one of the most important neurotransmitters in the nervous system, has been shown to be involved in various roles, such as learning and

Correspondence to: Prof. Chang-Jin Jeon, Neuroscience Lab., Department of Biology, College of Natural Sciences, Kyungpook National University, 80, Daehak-ro, Daegu, 41566, South Korea.
E-mail: cjjeon@knu.ac.kr

memory, arousal and attention, locomotor behavior, and neuronal plasticity [8, 9, 23, 25, 28, 63]. Cholinergic fibers have been found in the visual cortex of many mammals, including mice [43], rats [15, 48, 61], ferrets [30], cats [13, 66], monkeys [29], and humans [50]. However, only cholinergic neurons were found in the rat visual cortex [15, 61]. Cholinergic fibers, with abundant branches and varicosities, are distributed in all layers of the visual cortex. However, there are species differences in the higher density layers of cholinergic fibers in the visual cortex. For example, cats generally have dense cholinergic fibers in layer I, while in humans, cholinergic fibers are particularly intense in layers I, II, and the immediately adjacent rim of layer III. Cholinergic fiber synapses are predominantly symmetrical in the visual cortex, but a small number of asymmetries are observed [13, 61]. Cholinergic fibers are known to form synapses with GABAergic neurons, suggesting that acetylcholine indirectly inhibits visual information through GABAergic neurons [7, 16]. The visual cortex is known to receive cholinergic inputs from cholinergic neurons in the basal forebrain [6, 7, 19, 21, 51, 71, 74]. Among these, the nucleus of the diagonal band, the substantia innominata, and the nucleus basalis magnocellularis are well-known sources of cholinergic fibers in the visual cortex [11, 31, 33, 43, 49, 64, 74].

We previously reported the organization of the cholinergic system in the microbat central visual system, including the retina [59] and superior colliculus [38]. However, the distribution and morphology of cholinergic fibers have not been investigated in the microbat visual cortex. As part of a larger effort in our laboratory to localize cholinergic cells/fibers in the entire bat visual system [38, 59], the primary aim of the present study was to investigate the organization of the cholinergic system in the microbat visual cortex and compare it with other mammals, to understand the extent of species diversity. We also studied sources of cholinergic input into the visual cortex to determine whether the nocturnal microbat has a visual system similar to other predominantly diurnal mammalian species. Finally, we studied whether cholinergic fibers make contact with GABAergic interneurons. Our results contribute to a better understanding of the visual system of the nocturnal microbat.

II. Materials and Methods

Animal and tissue preparation

For this study, 12 freshly caught adult bats (*Rhinolophus ferrumequinum*, both sexes: 15–20 g) were used. All bats were captured in a cave in the district of Gimcheon, South Korea. After 5–6 hr to transport and stabilize the bats, they were anesthetized with a mixture of ketamine hydrochloride (30–40 mg/kg) and xylazine (3–6 mg/kg) prior to perfusion. The bats were perfused intracardially with 4% paraformaldehyde and 0.3–0.5% glutaraldehyde in 0.1 M sodium phosphate buffer (pH 7.4) containing 0.002% calcium chloride. Following a prerinse with approximately 30 ml of phosphate-buffered saline (PBS, pH 7.4) over a period of 3–5 min, each bat was perfused with 30–50 ml of fixative for 20–30 min via a syringe needle inserted through the left ventricle and aorta. The animal was decapitated and the head was placed in a fixative for 2–3 hr. The brain was then removed from the skull, stored for 2–3 hr in the same fixative and left overnight in 0.1 M phosphate buffer (pH 7.4) containing 8% sucrose and 0.002% calcium chloride. The brain was then mounted onto a chuck and cut into 50-μm thick coronal sections with a Vibratome 3000 Plus Sectioning System (Vibratome, St. Louis, MO, USA). All animal experiments were approved by the committee of Kyungpook National University (permission NO. 2016-0151). "Principles of laboratory animal care" (NIH publication No. 85-23, revised 1985) were followed.

Horseradish peroxidase staining

The primary antibody used in this study was goat anti-choline acetyltransferase (ChAT; Millipore, Bedford, MA, USA). Tissues were processed free-floating in small vials at room temperature with gentle agitation. For immunocytochemistry, tissues were incubated in 1% sodium borohydride ($NaBH_4$) for 30 min. Afterwards, these tissues were rinsed for 3 × 10 min in PBS, and incubated in PBS with 4% normal horse serum (Vector Laboratories, Burlingame, CA, USA) for 2 hr with 0.5% Triton X-100 added. The tissues were then incubated in the primary antiserum in PBS, with 4% normal serum for 24 hr, with 0.5% Triton X-100 added. The primary antiserum was diluted 1:200. Following three 10-min rinses in PBS, the tissues were incubated in a 1:200 dilution of biotinylated secondary IgG in a blocking solution. The secondary antibody used was biotinylated horse anti-goat (Vector Labs.). The tissues were then rinsed for 3 × 10 min in PBS and incubated in a 1:50 dilution of avidin-biotinylated horseradish peroxidase complex (Vector Labs.) in PBS for 2 hr. Then the tissues were rinsed in 0.25 M Tris buffer for 3 × 10 min. Finally, the staining was visualized by reacting with 1,3'-diaminobenzidine tetrahydrochloride (DAB) and hydrogen peroxide in 0.25 M Tris buffer for 3–10 min using a DAB reagent set (Kirkegaard & Perry, Gaithersburg, MD, USA). All tissues were then rinsed in 0.25 M Tris buffer before mounting. As a negative control, some sections were incubated in the same solution without the addition of the primary antibody, and these control tissues showed no ChAT immunoreactivity. Negative control and preabsorption tests for the specificity of this antibody conducted in the central nervous system of the microbat have been described in previous reports [38, 44]. Following the immunocytochemical procedures, the tissues were mounted on Superfrost Plus slides (Fisher, Pittsburgh, PA, USA) and dried overnight in a 37°C oven. The mounted sections were dehydrated, cleared, and coverslipped with Permount (Fisher).

Fluorescence immunohistochemistry

Standard triple-labeling immunohistochemical techniques and methods were used, as described previously [56]. The primary antibodies used for triple-labeling immunofluorescence were goat anti-ChAT (Millipore), mouse anti-GABA (Chemicon International Inc. Temecula, CA, USA), and rabbit anti-PSD-95 (Abcam, Cambridge, UK). Fluorescein-conjugated donkey anti-goat (Millipore), Cy3-conjucated donkey anti-mouse (Millipore), and Alexa fluor 674-conjucated donkey anti-rabbit (Millipore) were used as the secondary antibody. Stained sections were mounted on Superfrost Plus slides and coverslipped with Vectashield mounting medium (Vector Labs.). Immunofluorescence images were obtained using a laser-scanning confocal microscope (LSM 700; Carl Zeiss Meditec Inc. Jena, Germany).

Quantitative analysis

ChAT-IR fibers/cells were examined and photographed in the best-labeled sections from each of the three animals with a Zeiss Axioplan microscope, using conventional or differential interference contrast (DIC) optics. In addition, the average diameter/area of these cells were computed using an Axiocam HRc digital camera (Carl Zeiss Meditec Inc.). Analysis was performed using Zeiss AxioVision with Zeiss Plan-Apochromat objectives. To obtain the best image, bright and dark field microscopy was also used to identify the distribution pattern of ChAT-IR fibers, and only ChAT-IR cells containing a nucleus with a nucleolus that was at least faintly visible were included in the analysis. In addition, a standard for the fiber type was set up using the diameter of varicosity (small varicose fiber <0.5 μm, large varicose fiber >0.5 μm) [35, 38]. Images were adjusted with respect to brightness and contrast using Adobe Photoshop CS software (Adobe Systems Inc., San Jose, CA, USA). To quantify the density of IR fibers, we sampled sequential fields (total of nine tissue sections from three animals and three tissue sections from each animal), each 21 μm × 21 μm, across the superficial and deeper layers of the visual cortex. Lines indicating the IR fibers were generated with Adobe Photoshop. In order to quantify the laminar distribution of small and large immunoreactive varicosities (total of nine tissue sections from three animals and three tissue sections from each animal), we used a counting grid in the ocular of the microscope, which subtended 50 μm × 40 μm. We counted the number of varicosities within the grid in each layer. The grid was located in the middle of each layer and oriented perpendicular to the cortical surface.

Synaptic identification

The triple-labeling of ChAT-IR fibers, GABA, and PSD-95 were imaged using a laser-scanning confocal microscope module (Carl Zeiss Meditec Inc.) mounted on a fluorescence microscope. At the contact area of the ChAT fibers and GABA cells, the z-series of ChAT-IR fibers, GABA cell, and PSD-95 images were taken at 0.2 μm interval along the z-axis using a laser-scanning confocal microscope. The images were viewed using an EC Plan-Neofluar 10×, C-Apochromat 40×/1.2 W, and/or 100×/1.2 oil, objectives at 2.5× zoom. We obtained approximately 70–80 confocal images at the presumed synaptic contact. The z-series of the confocal images were reconstructed as three-dimensional (3D) images using the ZEN 2.3 (blue edition) program (Carl Zeiss Meditec Inc.). The 3D images and orthogonal views (xy, xz, and yz axes) were used to find points where the ChAT-IR fibers and PSD-95 made contact with the GABAergic cell.

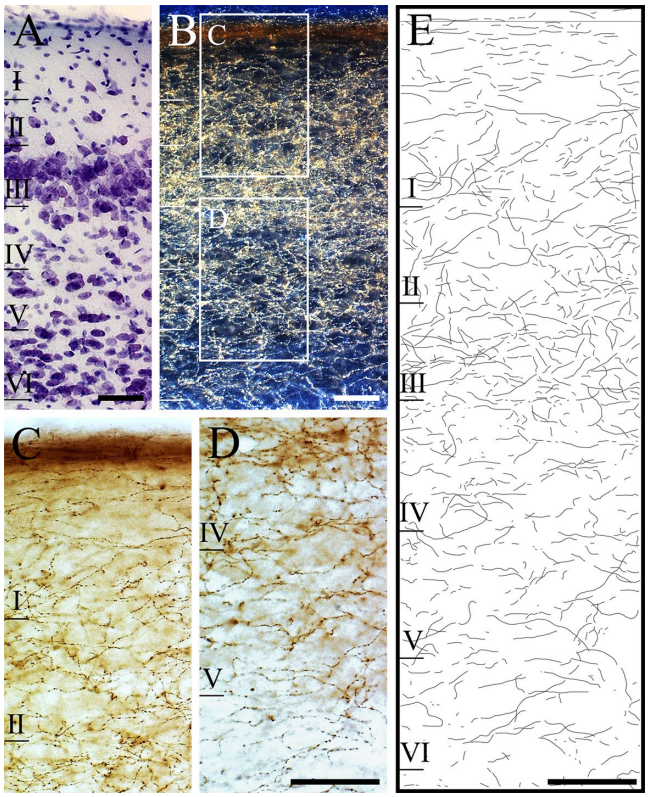

Fig. 1. Distribution of ChAT-IR fibers in the microbat visual cortex. (**A**) The approximate limits of layers are indicated in the thionin-stained section. (**B**) Low-magnification dark field photomicrograph of ChAT-IR fibers in the microbat visual cortex. (**C, D**) Medium magnification bright field photomicrograph of ChAT-IR fibers showing the areas marked in (**B**). Varicose cholinergic fibers generally observed in the microbat visual cortex. (**E**) Drawing of the ChAT-IR fibers in the microbat visual cortex. Bar = 50 μm.

III. Results

The distribution of ChAT-IR fibers in the microbat visual cortex

The laminar structure of the microbat visual cortex and the ChAT-immunoreactivity are shown in Figures 1A and 1B, respectively. These images demonstrate that the microbat visual cortex has well-developed cholinergic fibers. ChAT-IR fibers were distributed throughout all layers of the microbat visual cortex. Figures 1C and 1D show

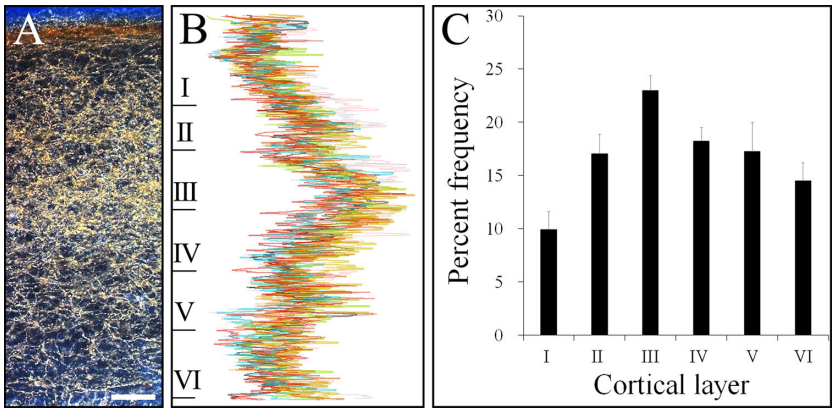

Fig. 2. Intensity profile of ChAT-IR fibers in the visual cortex of the microbat. In different coronal sections of the microbat visual cortex, a plot of the intensity of the ChAT-IR fibers characterized by the image processing program Image J developed at the National Institutes of Health. (**A**) Low-magnification dark field photomicrograph of ChAT-IR fibers in the microbat visual cortex shows well-labeled ChAT-IR fibers. (**B**) Results of intensity graph analyses from nine coronal sections of the microbat visual cortex are shown. (**C**) Density histogram of ChAT-IR fibers in the microbat visual cortex. The highest density of ChAT-IR fibers was located in layer III of the microbat visual cortex. Bar = 50 μm.

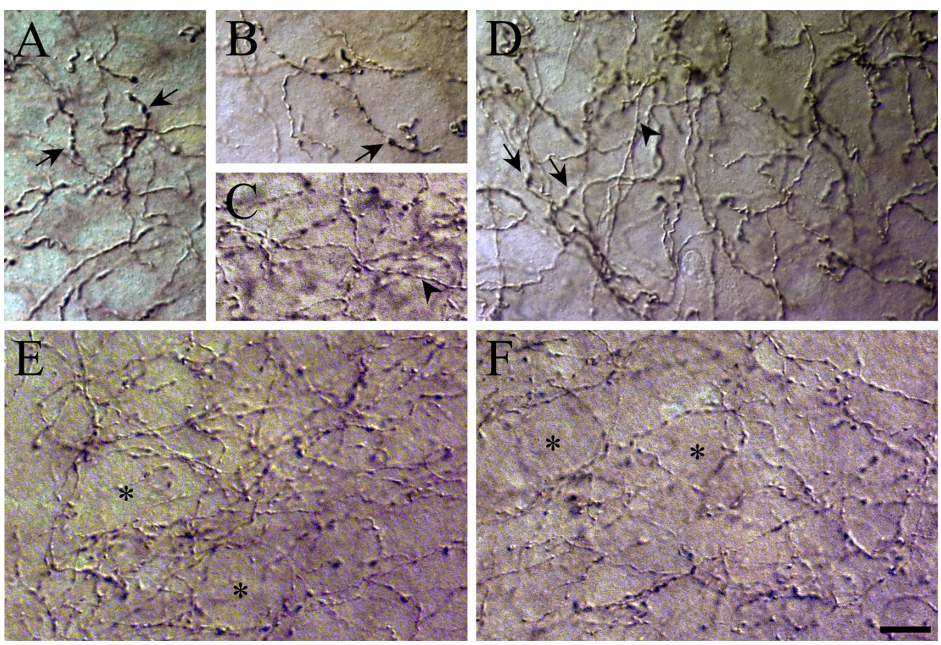

Fig. 3. High-power differential interference contrast (DIC) photomicrographs of ChAT-IR fibers in the microbat visual cortex. (**A, B**) Arrows indicate large varicosities in the microbat visual cortex. (**C**) Arrowheads indicate small varicosities in the microbat visual cortex. (**D**) ChAT-IR fibers with small (arrowheads) and large (arrows) varicosities in the microbat visual cortex. (**E, F**) Some ChAT-IR fibers surrounded unlabeled cells in the microbat visual cortex (asterisks in **E, F**). Bar = 10 μm.

highly magnified regions in the square areas of Figure 1B. Figure 1B is dark field figure, captured with a 20× objective, while Figure 1C, including ChAT-IR fibers located within layers I–III, and Figure 1D, showing ChAT-IR fibers located within layers IV–VI, are bright field figures, captured with a 40× objective. A drawing of the ChAT-IR fibers demonstrating their density is shown in Figure 1E. The cholinergic fibers in the microbat visual cortex reveal a plexus of labeled fibers with differential densities in the different layers. Quantitative maps of fiber distribution revealed the density of the ChAT-IR fibers in each layer (Fig. 2). Figure 2 also depicts the laminar distribution pattern of ChAT-IR fibers in the microbat visual cortex analyzed using the image processing program developed at the National Institute of Health. Three different sections taken from each of three different animals (a total of nine sections, each in a different color in Fig. 2C) were analyzed in the present study. Figure 2C shows a density histogram of ChAT-IR fibers in the microbat visual cortex. The frequency of labeled fibers varied in each layer. Thus, 9.95% of the labeled fibers appeared in layer I, 17.06% in layer II, 22.99% in layer III, 18.24% in layer IV, 17.24% in layer V,

Table 1. *Distribution of varicosities at different layers in three visual cortexes*

	Cortical layers					
	I	II	III	IV	V	VI
Small varicosities						
Visual cortex 1						
Number of varicosities	152	149	185	195	186	184
Density (varicosity/mm^2)	76167	74333	92500	97500	92833	92167
Visual cortex 2						
Number of varicosities	143	173	169	140	141	143
Density (varicosity/mm^2)	71500	86667	84333	70000	70333	71500
Visual cortex 3						
Number of varicosities	167	178	209	183	182	204
Density (varicosity/mm^2)	83667	88833	104333	91333	91167	101833
Total number (mean ± SD)	154.22 ± 27.97	166.56 ± 20.70	187.44 ± 33.29	172.56 ± 41.80	169.56 ± 38.30	177.00 ± 44.08
Density (mean ± SD)	77111.11 ± 13986.10	83277.80 ± 10350.48	93722.20 ± 16647.30	86277.80 ± 20904.70	84777.80 ± 19149.30	88500.00 ± 22044.00
Percentage	15.01 ± 2.75	16.21 ± 2.03	18.25 ± 0.91	16.80 ± 1.41	16.50 ± 1.64	17.23 ± 2.32
Large varicosities						
Visual cortex 1						
Number of varicosities	42	33	41	37	34	39
Density (varicosity/mm^2)	20833	16667	20667	18500	16833	19500
Visual cortex 2						
Number of varicosities	32	37	43	34	31	37
Density (varicosity/mm^2)	16167	18667	21833	17333	15667	18667
Visual cortex 3						
Number of varicosities	38	39	45	34	34	38
Density (varicosity/mm^2)	19167	19667	22500	17167	17000	19167
Total number (mean ± SD)	37.44 ± 9.28	36.67 ± 6.69	43.33 ± 3.54	35.33 ± 4.47	33.00 ± 4.87	38.22 ± 7.97
Density (mean ± SD)	18722.20 ± 4637.56	18333.30 ± 3344.77	21666.70 ± 2236.07	17666.70 ± 2236.07	16500.00 ± 2436.70	19111.10 ± 3982.60
Percentage	16.72 ± 2.02	16.37 ± 1.38	19.35 ± 1.97	15.77 ± 2.69	14.73 ± 2.51	17.06 ± 2.76

SD, standard deviation. * Number of varicosities = mean number from three tissue sections.

and 14.51% in layer VI. The highest density of ChAT-IR fibers occurred in layer III, while the lowest density of ChAT-IR fibers was located in layer I (Fig. 2B and 2C).

The morphology of ChAT-IR fibers in the microbat visual cortex

We identified at least two types of ChAT-IR varicose fibers in the microbat visual cortex. The first type of ChAT-IR varicose fibers was small varicose fibers (arrowheads in Fig. 3C and 3D), and the second type was large varicose fibers (arrows in Fig. 3A, 3B, and 3D). Varicose fibers were distributed throughout the rostrocaudal section of the microbat visual cortex and numerous ChAT-IR varicosities were distributed irregularly along the fibers. ChAT-IR fibers in the microbat visual cortex exhibited various orientations, including vertical, horizontal, and oblique orientations. Some ChAT-IR fibers surrounded unlabeled somata in the microbat visual cortex (indicated by asterisks) (Fig. 3E and 3F). The microbat visual cortex does not appear to have cholinergic neurons; no labeled neurons were found in the present study.

Figure 4 and Table 1 show the distributional difference of small and large varicosities in the microbat visual cortex. The distribution of large varicosities in each layer was as follows: 37.44 ± 9.28 (16.72%; mean ± standard deviation [SD]) in layer I, 36.67 ± 6.69 (16.37%; mean ± SD) in layer II, 43.33 ± 3.54 (19.34%; mean ± SD) in layer III, 35.33 ± 4.47 (15.77%; mean ± SD) in layer IV, 33.00 ± 4.87 (14.73%; mean ± SD) in layer V, and 38.22 ± 7.97 (17.06%; mean ± SD) in layer VI. Although the density of the large varicosities was not highly different in each layer, the highest density of large varicosities occurred in layer

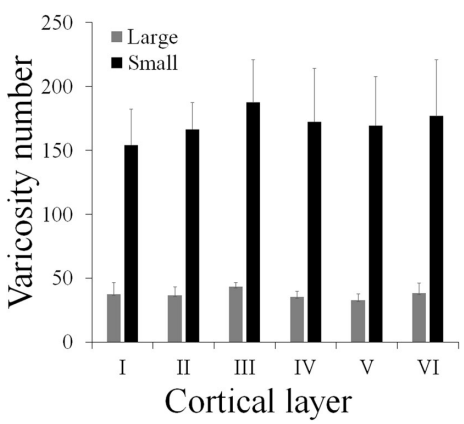

Fig. 4. Histogram of the distribution of two types of varicosities in the microbat visual cortex. Although there were not many differences, the layer III contained higher number of both large and small varicosities than other layers. In each layer, there were more small varicosities than large ones. The microbat visual cortex contained 4.59 times more small varicosities than large ones.

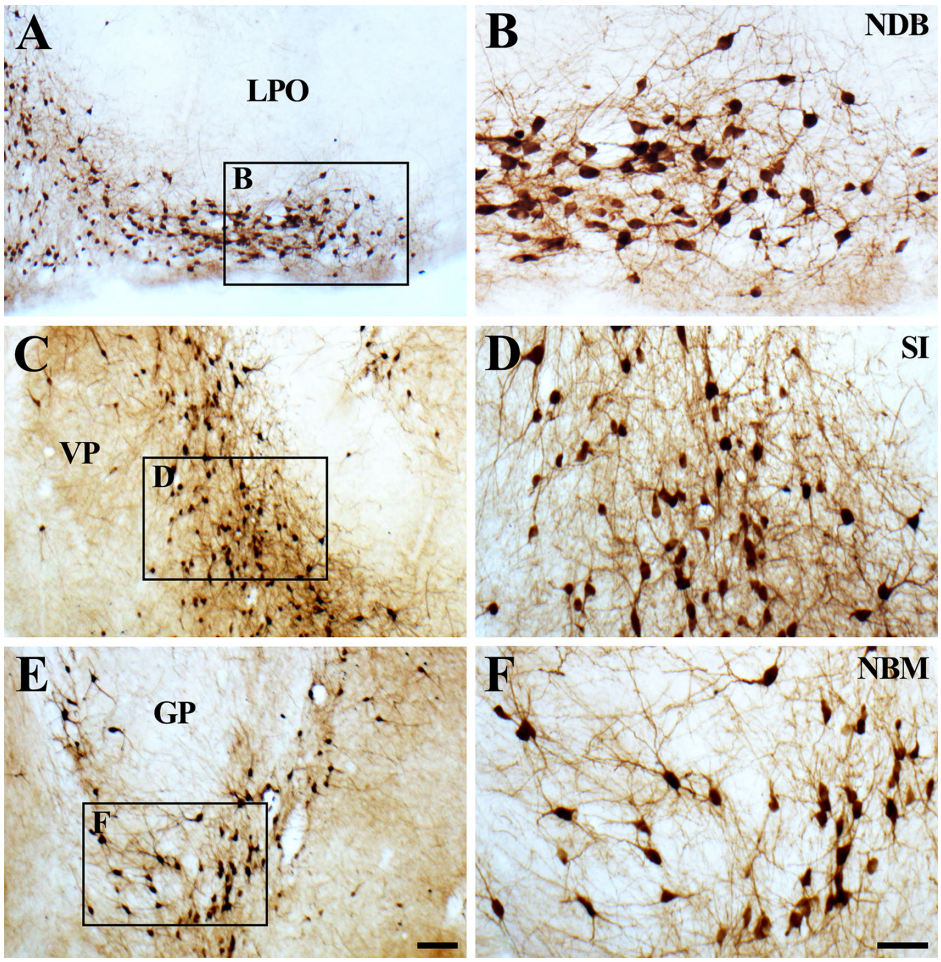

Fig. 5. Photomicrographs showing presumed sources of ChAT-IR fibers in the microbat visual cortex. (**A**) Low-magnification photomicrograph of coronal sections showing the nucleus of the diagonal band. (**B**) High-magnification photomicrograph of image in the square marked in (**A**). (**C**) Low magnification photomicrograph of a coronal section showing the substantia innominata. (**D**) High magnification photomicrograph of image in the square marked in (**C**). (**E**) Low-magnification photomicrograph of a coronal section showing the nucleus basalis magnocellularis. (**F**) High-magnification photomicrograph of image in the square marked in (**E**). LPO, lateral preoptic area; NDB, nucleus of the diagonal band; VP, ventral pallidum; SI, substantia innominata; GP, Globus pallidus; NBM, nucleus basalis magnocellularis. Bar = 200 μm (**A, C, E**), and 50 μm (**B, D, F**).

III. The distribution of small varicosities in each layer was as follows: 154.22 ± 27.97 (15.05%; mean ± SD) in layer I, 166.56 ± 20.70 (16.21%; mean ± SD) in layer II, 187.44 ± 33.29 (18.25%; mean ± SD) in layer III, 172.56 ± 41.80 (16.80%; mean ± SD) in layer IV, 169.56 ± 38.30 (16.50%; mean ± SD) in layer V, and 177.00 ± 44.08 (17.23%; mean ± SD) in layer VI. The highest density of small varicosities also occurred in layer III. Small varicosities were 4.59 times more than large varicosities in the microbat visual cortex.

The sources of ChAT-IR fibers in the microbat visual cortex

There are several subdivisions of cholinergic neurons in the central nervous system. The predominant groups of cholinergic neurons observed in the brain are found in the striatum, basal forebrain, diencephalon, pons, and cranial nerve nuclei [4, 47, 73, 74]. The nucleus basalis magnocellularis, the substantia innominata, and the nucleus of the diagonal band are known to project cholinergic fibers into the visual cortex [11, 31, 33, 43, 49, 64, 74].

1) Nucleus of diagonal band

ChAT-IR neurons were distributed in the horizontal diagonal band of the bat brain (Fig. 5A and 5B) [14, 44, 47]. The labeling of ChAT-IR neurons was intense in various types of neurons in the horizontal diagonal band. The large majority of ChAT-IR neurons were round/oval cells (Fig. 6A), although other cell types were also observed, including pyriform (Fig. 6B) and horizontal cells (Fig. 6C). The average diameter of 86 ChAT-IR neurons in the horizontal diagonal band ranged from 11.8 to 20.21 μm, with a mean of 16.13 μm (SD = 2.00 μm). The area of these cells ranged from 109.31 to 320.8 μm^2, with a mean of 207.46 μm^2 (SD = 50.05 μm^2) (Fig. 7 and Table 2).

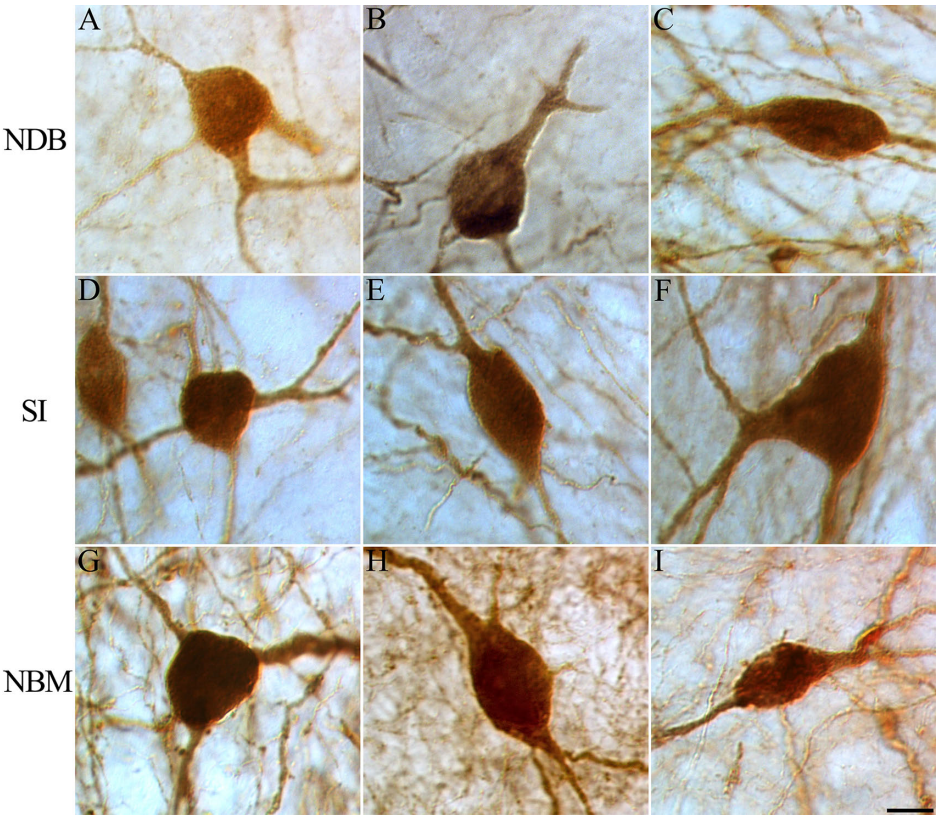

Fig. 6. High-power differential interference contrast (DIC) photomicrographs of major ChAT-IR cell types in the nucleus of the diagonal band, substantia innominata and the nucleus basalis magnocellularis of microbat. (**A**) A multipolar round cell with several processes in various directions. (**B**) A pyriform cell. (**C**) A horizontal fusiform cell with a horizontal fusiform cell body and horizontally oriented processes. (**D**) A multipolar round cell. (**E**) A vertical fusiform cell with a vertical fusiform cell body and vertically oriented processes. (**F**) A large multipolar stellate cell. (**G**) A multipolar round cell. (**H**) A vertical fusiform cell with a vertical fusiform cell body and vertically oriented processes. (**I**) A horizontal fusiform cell with a horizontal fusiform cell body and horizontally oriented processes. NDB, nucleus of the diagonal band; SI, substantia innominata; NBM, nucleus basalis magnocellularis. Bar = 5 μm.

Table 2. *Quantitative data of choline acetyltransferase-immunoreactive cells in the microbat nucleus of the diagonal band, substantia innominata, and nucleus basalis magnocellularis*

	Animal number	Number of ChAT-IR cells	Diameter ± SD (μm)	Area ± SD (μm^2)
Nucleus of the diagonal band	1	31	15.08 ± 1.54	180.45 ± 36.06
	2	34	16.49 ± 1.92	216.41 ± 48.89
	3	21	16.81 ± 2.18	225.53 ± 56.16
	Total/Average	86	16.12 ± 2.00	207.46 ± 50.05
Substantia innominata	1	35	12.41 ± 1.67	123.13 ± 33.64
	2	35	13.16 ± 1.95	138.84 ± 40.34
	3	28	14.54 ± 2.11	169.54 ± 50.41
	Total/Average	98	13.37 ± 2.00	143.84 ± 45.00
Nucleus basalis magnocellularis	1	31	13.50 ± 2.02	146.12 ± 43.29
	2	31	14.23 ± 1.59	161.19 ± 35.13
	3	28	13.95 ± 1.67	153.06 ± 37.15
	Total/Average	90	13.90 ± 1.78	153.46 ± 38.81

ChAT-IR, choline acetyltransferase-immunoreactive; SD, standard deviation.

2) Substantia innominata

ChAT-IR neurons appeared in various shapes in the substantia innominata (Fig. 5C and 5D). The major type of neurons found in the substantia innominata were medium sized round/oval cells (Fig. 6D). However, many vertical fusiform cells (Fig. 6E) and stellate cells (Fig. 6F) were also IR for ChAT. The average diameter of 98 ChAT-IR neurons in the substantia innominata ranged from 8.33 to

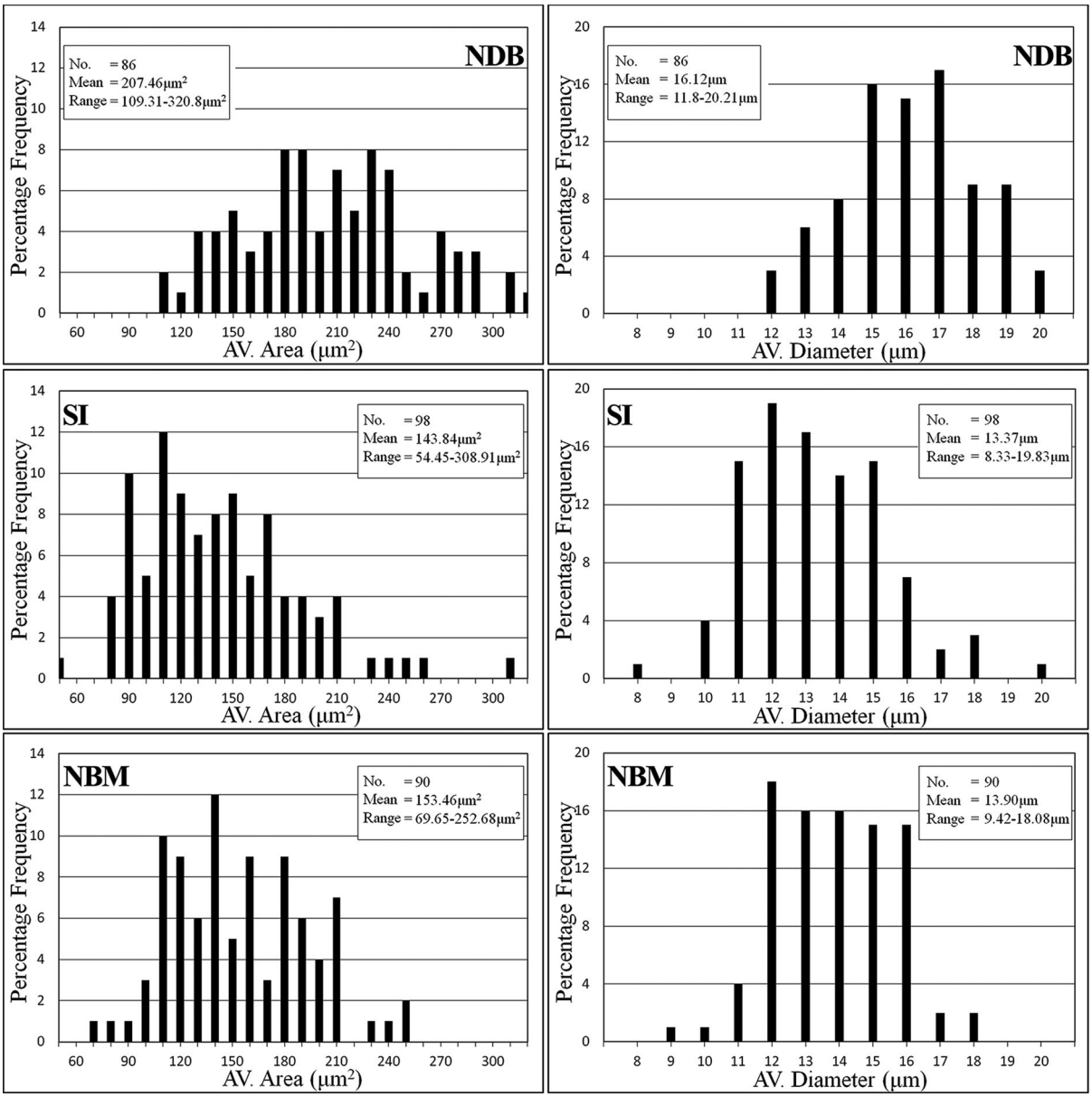

Fig. 7. Histogram of ChAT-IR cell area and diameter in the microbat brain. The diameter of 86 ChAT-IR neurons in the horizontal diagonal band ranged from 11.8 to 20.21 μm, with a mean of 16.13 μm (standard deviation, S.D. = 2.00 μm). The area of these cells ranged from 109.31 to 320.8 μm^2, with a mean of 207.46 μm^2 (S.D. = 50.05 μm^2). The average diameter of 98 ChAT-IR neurons in the substantia innominata ranged from 8.33 to 19.83 μm, with a mean of 13.37 μm (S.D. = 2.00 μm). The area of these cells ranged from 54.45 to 308.91 μm^2, with a mean of 143.84 μm^2 (S.D. = 45 μm^2). The diameter of 90 ChAT-IR neurons in the nucleus basalis magnocellularis ranged from 11.77 to 18.08 μm, with a mean of 13.90 μm (S.D. = 1.78 μm). The area of these cells ranged from 108.72 to 252.68 μm^2, with a mean of 153.46 μm^2 (S.D. = 38.81 μm^2). The best-stained cells were measured. NDB, nucleus of the diagonal band; SI, substantia innominata; NBM, nucleus basalis magnocellularis.

19.83 μm, with a mean of 13.37 μm (SD = 2.00 μm). The area of these cells ranged from 54.45 to 308.91 μm^2 with a mean of 143.84 μm^2 (SD = 45 μm^2) (Fig. 7 and Table 2).

3) Nucleus basalis magnocellularis

ChAT-IR neurons were intense among various types of cells in the nucleus basalis magnocellularis (Fig. 5E and 5F). The large majority of ChAT-IR neurons were round/oval (Fig. 6G), vertical fusiform (Fig. 6H), and horizontal cells (Fig. 6I), although other cell types were also observed, including stellate and pyriform cells. The average diameter of 90 ChAT-IR neurons in the nucleus basalis magnocellularis ranged from 11.77 to 18.08 μm, with a mean of 13.90 μm (SD = 1.78 μm). The area of these cells ranged from 108.72 to 252.68 μm^2, with a mean of 153.46 μm^2 (SD = 38.81 μm^2) (Fig. 7 and Table 2).

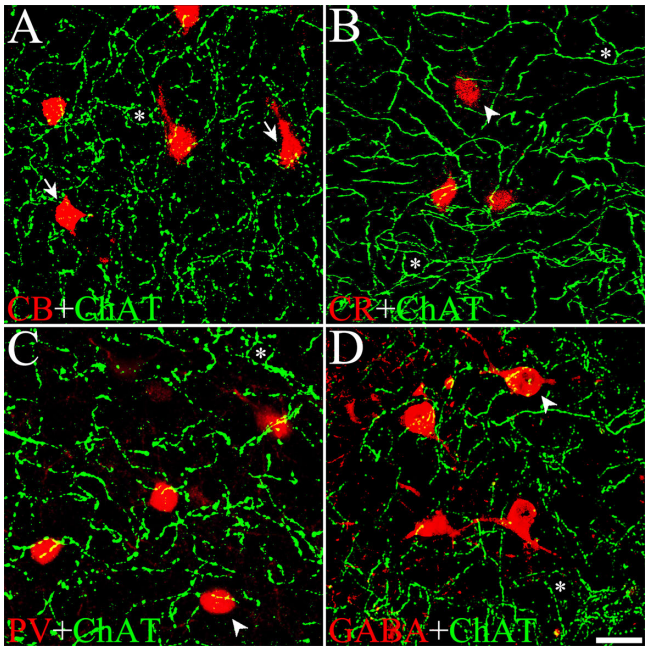

Fig. 8. Double labeling of ChAT-IR fibers with CB-, CR-, PV- or GABA-IR cells in the microbat visual cortex. (**A**) Merged image of fluorescence-reacted ChAT-IR fibers and CB-IR cells. (**B**) Merged image of fluorescence-reacted ChAT-IR fibers and CR-IR cells. (**C**) Merged image of fluorescence-reacted ChAT-IR fibers and PV-IR cells. (**D**) Merged image of fluorescence-reacted ChAT-IR fibers and GABA-IR cells. Some round/oval (arrowheads) cells in **B, C, D**, or stellate cells (arrows) in **A**. However, we did not detect CB-, CR-, PV-, or GABA-IR cells surrounded by the ChAT-IR fibers (asterisks). ChAT, Choline acetyltransferase; CB, calbindin-D28K; CR, calretinin; PV, parvalbumin; GABA, gamma-aminobutyric acid. Bar = 20 μm.

The distribution of ChAT-IR fibers and CB-, CR-, PV-, or GABA-IR cells

Among the many calcium-binding proteins (CBP), calbindin-D28K (CB), calretinin (CR), and parvalbumin (PV) are important markers for specific neuronal subpopulations in the central nervous system [2, 5]. CB, CR, and PV are localized in the visual cortex of various mammals [20, 34, 46, 60]. In a previous study, we showed that many round/oval and stellate cells in the microbat visual cortex contained CB, CR, or PV, and many of these cells also contained GABA [41]. In the present study, some ChAT-IR fibers surrounded unlabeled somata in the microbat visual cortex (asterisks, Fig. 3E and 3F). Figure 8 shows that CB-, CR-, PV- or GABA-IR appears in some round/oval (arrowheads) or stellate cells (arrows) in the microbat visual cortex. However, we did not detect any CB-, CR-, PV-, or GABA-IR cells surrounded by ChAT-IR fibers (asterisks).

Triple-labeling of ChAT-IR fibers, PSD-95 and GABA

In the present study, we performed triple labeling of ChAT-IR fibers, PSD-95, and GABA, in order to identify the synaptic contacts of ChAT-IR fibers with GABA-IR cells. Figure 9 shows the distribution of ChAT-IR fibers (Fig. 9A, green), GABA (Fig. 9B, red), PSD-95 (Fig. 9C, blue), and a merged image (Fig. 9D), in the microbat visual cortex. The crosshair reveals the colocalization of ChAT-IR fibers and PSD-95 with the GABA-IR cells, in an orthogonal projection. The areas marked by white squares in Figures 9A–D are displayed at higher magnification in Figures 9E–P. Figure 9E, 9I, and 9M show merged images of fluorescence ChAT-IR fibers and GABA-IR cells in the xy, xz, and yz planes, respectively. With this method, we identified that ChAT-IR fibers coincided with GABA-IR cells. Figures 9F, 9J, and 9N show merged images of fluorescence ChAT-IR fibers and PSD-95-IR puncta in the xy, xz, and yz planes, respectively. These figures show that ChAT-IR fibers coincided with PSD-95 puncta. Figures 9G, 9K, and 9O show merged images of fluorescence GABA-IR cells and PSD-95 puncta in xy, xz, and yz planes, respectively. These figures demonstrate the coincidence of GABA-IR cells with PSD-95 puncta. Figures 9H, 9L, and 9P show merged images of fluorescence ChAT-IR fibers, PSD-95, and GABA-IR cells. The merged images show that ChAT-IR fibers make contact with GABA-IR cell in the microbat visual cortex.

IV. Discussion

This study has demonstrated that ChAT-IR fibers are distributed in the microbat visual cortex. However, the distribution pattern of these fibers is rather different from that found in previous studies on the visual cortex in other mammals. We identified at least two types of ChAT-IR varicose fibers in the present study. ChAT-IR cells in the basal forebrain areas that are thought to be the source of ChAT-IR in the visual cortex were also identified. Some of the ChAT-IR fibers contacted GABAergic neurons.

Cholinergic fibers have been found in the visual cortex of numerous mammals, including mice [43], rats [15, 48, 61], ferrets [30], cats [13, 66], monkeys [29], and humans [50]. However, there are species differences in the distribution pattern of cholinergic fibers in the visual cortex among the various animals. For example, dense cholinergic fibers are distributed in layer IV of the mouse visual cortex [43], while dense cholinergic fibers are found in layer IV of male Long-Evans rats' [15] or in layer V of Sprague-Dawley albino rats' [61] visual cortex. A low density of cholinergic fibers is found in layer IV of the ferret visual cortex [30], while cholinergic fibers are particularly dense in layer I of the cat visual cortex [13, 66]. In the monkey visual cortex, dense cholinergic fibers are distributed in layers I and IV [29]. In the human visual cortex, cholinergic fibers are particularly intense in layers I, II, and the immediately adjacent rim of layer III [50]. In contrast, in the present study, the highest density of cholinergic fibers was distributed in layer III, while the lowest density of cholinergic fibers was located in layer I in the microbat visual cortex. Thus, the combined results of the previous and the present studies indicate that different animals possess different density of cholinergic fibers among the six layers of the visual cortex.

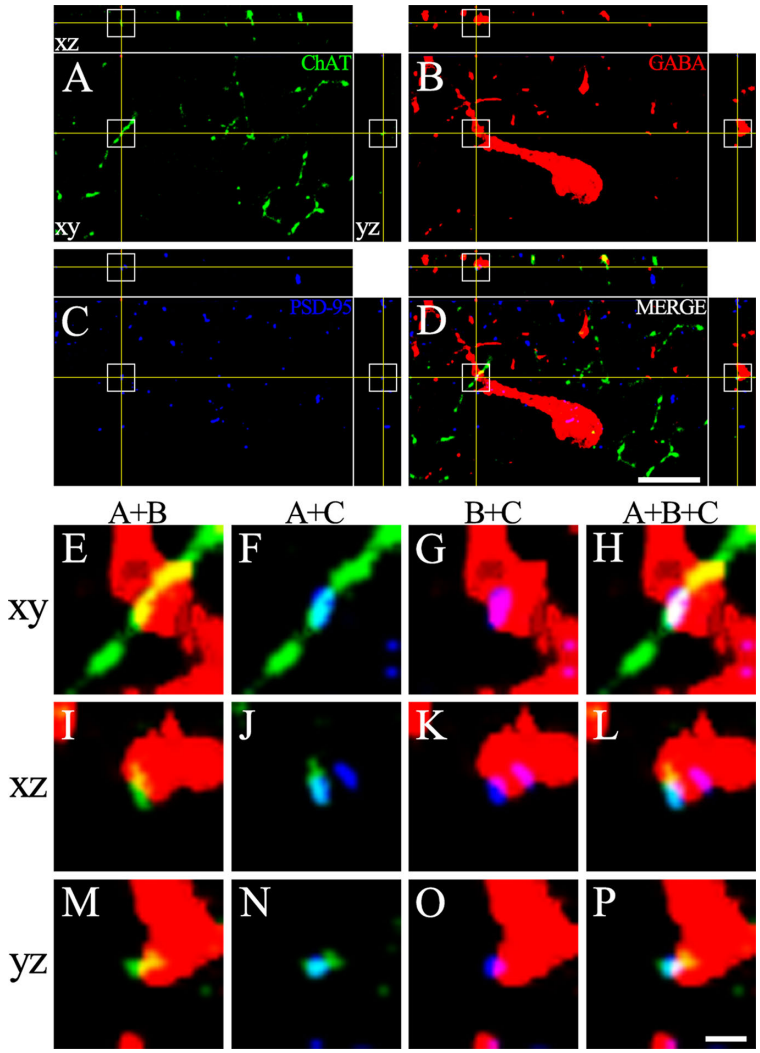

Fig. 9. Triple-labeled image of ChAT-IR fibers, GABA and PSD-95 in the microbat visual cortex. (**A**) Orthogonal view of a confocal z-stack image of the ChAT-IR fibers (green). (**B**) Orthogonal view of a confocal z-stack image of the GABA-IR cells (red). (**C**) Orthogonal view of a confocal z-stack image of PSD-95 IR (blue). (**D**) Orthogonal view of a confocal z-stack image of the merged images. (**E–P**) High-power images in crosshair from the xy, xz, and yz planes, respectively. (**E, I, M**) Merged images of fluorescence ChAT-IR fibers and PSD-95 puncta in the xy, xz, and yz planes, respectively. (**F, J, N**) Merged images of fluorescence ChAT-IR fibers and GABA-IR cell in the xy, xz, and yz planes, respectively. (**G, K, O**) Merged images of fluorescence GABA-IR cell and PSD-95 puncta in the xy, xz, and yz planes, respectively. (**H, L, P**) Merged images of fluorescence ChAT-IR fibers, PSD-95, and GABA-IR cell in the xy, xz, and yz planes, respectively. ChAT, Choline acetyltransferase; GABA, gamma-aminobutyric acid. Bar = 10 μm (**A–D**); 1 μm (**E–P**).

The functional significance of inter-species differences in the density distribution of cholinergic fibers in the visual cortex of mammals remains unknown.

In the present study, ChAT-IR neurons were not found in the microbat visual cortex. This result is in accordance with the majority of previous results from other mammalian visual cortex studies. Thus, no ChAT-IR neurons were found in the visual cortex of mice [43], ferrets [30], cats [13, 66], or humans [50]. In contrast, however, the rat visual cortex was found to contain ChAT-IR neurons [15, 48, 61]. ChAT-IR neurons were observed in layers II-VI of the rat visual cortex. Most of these neurons were either round or oval in shape and small in size. The large majority of ChAT-IR neurons were bipolar cells [15, 48, 61]. However, the functional role of cholinergic cells in the rat visual cortex has not yet been described.

Several studies have shown that cholinergic fiber inputs to the neocortex initiate primarily from cholinergic neurons of the basal forebrain [6, 7, 19, 21, 51, 71, 74]. In the forebrain, the nucleus basalis magnocellularis, substantia innominata, and the nucleus of the diagonal band are known to project cholinergic fibers to the visual cortex [11, 31, 33, 43, 49, 64, 74]. In previous studies in bats, ChAT immunoreactivity was found in the basal forebrain areas [14, 44, 47]. In the present study, in the nucleus of the diagonal band, soma diameters varied from 11.8–20.21 μm (mean diameter 16.12 μm) and the predominant type of ChAT-IR cell was round or oval. In the substantia innomi-

nata, soma diameters varied from 8.33–19.83 μm (mean diameter 13.37 μm) and the predominant type of ChAT-IR cell was round or oval. In the nucleus basalis magnocellularis, soma diameters varied from 9.42–18.08 μm (mean diameter 13.90 μm) and the predominant type of ChAT-IR cell was also round or oval in shape. These results suggest that, although the cholinergic inputs can be confirmed by retrograde tracer injection, cholinergic round/oval cells of various sizes project to the microbat visual cortex, giving rise to different sizes of cholinergic fibers in microbat visual cortex.

In the present study, ChAT-IR varicosities were found throughout the microbat visual cortex. Varicose cholinergic fibers are a common characteristic found in many other mammals. For instance, varicose cholinergic fibers were found in mice [43], rats [15, 48, 61], ferrets [30], cats [13, 66], and humans [50]. In the present study, we found at least two different types of fibers, small and large varicose fibers, in the microbat visual cortex. Two types of ChAT-IR synaptic profiles were observed in the cat superior colliculus using electron microscopy. Small-diameter fibers with few varicosities contained predominantly round synaptic vesicles and formed asymmetric synaptic contacts, while large-diameter fibers with many varicosities also contained round synaptic vesicles and formed symmetric synaptic contacts. These two types of fibers were found only in the superficial layers of the cat superior colliculus and the large fibers were not found in the deeper layers of the superior colliculus [35]. Two types of ChAT-fibers were also found in the microbat superior colliculus [38]. In the microbat superior colliculus, however, the two different types of fibers were found in both superficial and deeper layers. Electron microscopy studies confirmed that the ChAT-IR varicose profiles in the visual cortex contained round synaptic vesicles forming symmetric and asymmetric synaptic complexes in cat [13], and rat [61]. These results suggest that synapses can be made in the varicose fibers of the microbat visual cortex. However, electron microscopy studies will be required to confirm the synaptic profiles of the ChAT-IR fibers in the bat visual cortex.

Previous studies have shown that GABAergic neurons receive more ChAT-IR fiber input than non-GABAergic neurons and most cholinergic boutons formed synapses with dendritic shafts of GABAergic neurons in the cat visual cortex [7]. Beaulieu and Somogyi [7] suggested that "The activation of GABAergic neurons by cholinergic afferents may increase the response specificity of cortical cells during cortical arousal thought to be mediated by the basal forebrain". The inhibitory effect of cholinergic fibers is thought to be indirectly mediated by activation of GABAergic neurons in the visual cortex [7]. Muscarinic acetylcholine receptors were found in the GABAergic neurons in the cat visual cortex [16]. In the present study, we found that cholinergic fibers make contact with GABAergic neurons in the microbat visual cortex. This suggests that cholinergic fibers in the visual cortex of microbats may also have an indirect inhibitory effect through muscarinic acetylcholine receptors on GABAergic neurons. However, additional physiological and pharmacological studies will be required to identify the functional role of acetylcholine in the visual cortex of microbats.

The cholinergic system is known to play a key role in the central nervous system. Behavioral and physiological regulation including sensory processing, learning, memory, neural plasticity, mood, sleep, arousal, biorhythms, and attention, are regulated by acetylcholine [8, 23, 25, 28, 63]. In the visual cortex, ACh has also been implicated in neural plasticity, attention and learning. For example, ACh plays a role in facilitation of perceptual learning via attention [40] and in regulation of learning to discriminate fine differences in the temporal stimuli [52]. ACh contributes to experience-dependent synaptic plasticity in visual cortex [25]. In addition, ACh plays a role in regulating the strength of the thalamo-cortical inputs leading to the selection and/or discrimination of visual stimuli [45]. A recent study showed that ACh also participates in improvement of visuospatial perception and processing of visual targets among distractors [24]. Thus, our results show a well-organized cholinergic system in the microbat visual cortex, suggesting that cholinergic fibers in the microbat visual cortex may play a role in synaptic plasticity, attention, and arousal, and improve the signal-to-noise ratio of cortical neurons during visual information processing [24, 25, 40, 45, 52]. However, determining the detailed functional role of cholinergic fibers in the microbat visual cortex requires electrophysiological studies.

In conclusion, we found well-organized ChAT-IR fibers in the microbat visual cortex, with the highest density in layer III. However, ChAT-IR cells were not observed in the microbat visual cortex. The nucleus of the diagonal band, substantia innominata, and nucleus basalis magnocellularis, which are known as sources of cholinergic fibers in the mammalian visual cortex, contained many well-labelled ChAT-IR neurons in the microbat visual cortex. The study also confirmed that some ChAT-IR fibers were in contact with GABAergic neurons. Our study provides important information contributing to better understanding of the visual system of the nocturnal mammal microbat, which has previously been thought to have an atrophied visual system.

V. Conflicts of Interest

The authors declare that there are no conflicts of interest.

VI. Acknowledgment

We thank Cactus Communications for proofreading the manuscript. This research was supported by the Basic Science Research Program through the National Research Foundation of Korea (NRF), funded by the Ministry of Education (NRF2016R1D1A1A09918427).

VII. References

1. Adams, R. A. (2000) Wing ontogeny, shifting niche dimensions, and adaptive landscapes. In "Ontogeny, Functional Ecology, and Evolution of Bats", ed. by R. A. Adams and S. C. Pedersen, Cambridge University Press, Cambridge, pp. 275–315.
2. Alexianu, M. E., Ho, B. K., Mohamed, A. H., La Bella, V., Smith, R. G. and Appel, S. H. (1994) The role of calcium-binding proteins in selective motoneuron vulnerability in amyotrophic lateral sclerosis. *Ann. Neurol.* 36; 846–858.
3. Altringham, J. D. (1996) Bats: Biology and Behaviour. Oxford University Press, New York.
4. Armstrong, D. M., Saper, C. B., Levey, A. I., Wainer, B. H. and Terry, R. D. (1983) Distribution of cholinergic neurons in rat brain: demonstrated by the immunocytochemical localization of choline acetyltransferase. *J. Comp. Neurol.* 216; 53–68.
5. Baimbridge, K. G., Celio, M. R. and Rogers, J. H. (1992) Calcium-binding proteins in the nervous system. *Trends Neurosci.* 15; 303–308.
6. Bear, M. F., Carnes, K. M. and Ebner, F. F. (1985) An investigation of cholinergic circuitry in cat striate cortex using acetylcholinesterase histochemistry. *J. Comp. Neurol.* 234; 411–430.
7. Beaulieu, C. and Somogyi, P. (1991) Enrichment of cholinergic synaptic terminals on GABAergic neurons and coexistence of immunoreactive GABA and choline acetyltransferase in the same synaptic terminals in the striate cortex of the cat. *J. Comp. Neurol.* 304; 666–680.
8. Blokland, A. (1995) Acetylcholine: a neurotransmitter for learning and memory? *Brain Res. Brain Res. Rev.* 21; 285–300.
9. Bucci, D. J., Holland, P. C. and Gallagher, M. (1998) Removal of cholinergic input to rat posterior parietal cortex disrupts incremental processing of conditioned stimuli. *J. Neurosci.* 18; 8038–8046.
10. Butz, E., Peichl, L. and Müller, B. (2015) Cone bipolar cells in the retina of the microbat Carollia perspicillata. *J. Comp. Neurol.* 523; 963–981.
11. Carey, R. G. and Rieck, R. W. (1987) Topographic projections to the visual cortex from the basal forebrain in the rat. *Brain Res.* 424; 205–215.
12. Covey, E. (2005) Neurobiological specializations in echolocating bats. *Anat. Rec. A Discov. Mol. Cell. Evol. Biol.* 287; 1103–1116.
13. De Lima, A. D. and Singer, W. (1986) Cholinergic innervation of the cat striate cortex: A choline acetyltransferase immunocytochemical analysis. *J. Comp. Neurol.* 250; 324–338.
14. Dell, L. A., Kruger, J. L., Bhagwandin, A., Jillani, N. E., Pettigrew, J. D. and Manger, P. R. (2010) Nuclear organization of cholinergic, putative catecholaminergic and serotonergic systems in the brains of two megachiropteran species. *J. Chem. Neuroanat.* 40; 177–195.
15. Eckenstein, F. P., Baughman, R. W. and Quinn, J. (1988) An anatomical study of cholinergic innervation in rat cerebral cortex. *Neuroscience* 25; 457–474.
16. Erisir, A., Levey, A. I. and Aoki, C. (2001) Muscarinic receptor M(2) in cat visual cortex: Laminar distribution, relationship to gamma aminobutyric acidergic neurons, and effect of cingulate lesions. *J. Comp. Neurol.* 441; 168–185.
17. Feller, K. D., Lagerholm, S., Clubwala, R., Silver, M. T., Haughey, D., Ryan, J. M., Loew, E. R., Deutschlander, M. E. and Kenyon, K. L. (2009) Characterization of photoreceptor cell types in the little brown bat Myotis lucifugus (Vespertilionidae). *Comp. Biochem. Physiol. B, Biochem. Mol. Biol.* 154; 412–418.
18. Fenton, M. B. and Simmons, N. B. (2014) Bats: A World of Science and Mystery. University of Chicago Press, Chicago.
19. Fibiger, H. C. (1982) The organization and some projections of cholinergic neurons of the mammalian forebrain. *Brain Res.* 257; 327–388.
20. Gao, W. J., Wormington, A. B., Newman, D. E. and Pallas, S. L. (2000) Development of inhibitory circuitry in visual and auditory cortex of postnatal ferrets: immunocytochemical localization of calbindin- and parvalbumin-containing neurons. *J. Comp. Neurol.* 422; 140–157.
21. Gielow, M. R. and Zaborszky, L. (2017) The input-output relationship of the cholinergic basal forebrain. *Cell Rep.* 18; 1817–1830.
22. Glezer, I. I., Hof, P. R., Leranth, C. and Morgane, P. J. (1993) Calcium-binding protein-containing neuronal populations in mammalian visual cortex: a comparative study in whales, insectivores, bats, rodents, and primates. *Cereb. Cortex* 3; 249–272.
23. Gold, P. E. (2003) Acetylcholine modulation of neural systems involved in learning and memory. *Neurobiol. Learn. Mem.* 80; 194–210.
24. Gratton, C., Yousef, S., Aarts, E., Wallace, D. L., D'Esposito, M. and Silver, M. A. (2017) Cholinergic, but not dopaminergic or noradrenergic, enhancement sharpens visual spatial perception in humans. *J. Neurosci.* 37; 4405–4415.
25. Gu, Q. (2003) Contribution of acetylcholine to visual cortex plasticity. *Neurobiol. Learn. Mem.* 80; 291–301.
26. Gu, Y. N., Kim, H. G. and Jeon, C. J. (2015) Localization of nitric oxide synthase-containing neurons in the bat visual cortex and co-localization with calcium-binding proteins. *Acta Histochem. Cytochem.* 48; 125–133.
27. Gutierrez Ede, A., Pessoa, V. F., Aguiar, L. M. and Pessoa, D. M. (2014) Effect of light intensity on food detection in captive great fruit-eating bats, Artibeus lituratus (Chiroptera: Phyllostomidae). *Behav. Processes* 109; 64–69.
28. Haam, J. and Yakel, J. L. (2017) Cholinergic modulation of the hippocampal region and memory function. *J. Neurochem.* 2; 111–121.
29. Hedreen, J. C., Uhl, G. R., Bacon, S. J., Fambrough, D. M. and Price, D. L. (1984) Acetylcholinesterase-immunoreactive axonal network in monkey visual cortex. *J. Comp. Neurol.* 226; 246–254.
30. Henderson, Z. (1987) Cholinergic innervation of ferret visual system. *Neuroscience* 20; 503–518.
31. Henderson, Z. (1987) Source of cholinergic input to ferret visual cortex. *Brain Res.* 412; 261–268.
32. Holland, R. A., Waters, D. A. and Rayner, J. M. (2004) Echolocation signal structure in the Megachiropteran bat Rousettus aegyptiacus Geoffroy 1810. *J. Exp. Biol.* 207; 4361–4369.
33. Huppé-Gourgues, F., Jegouic, K. and Vaucher, E. (2018) Topographic organization of cholinergic innervation from the basal forebrain to the visual cortex in the rat. *Front. Neural. Circuits.* 8; 12–19.
34. Ichida, J. M., Rosa, M. G. and Casagrande, V. A. (2000) Does the visual system of the flying fox resemble that of primates? The distribution of calcium-binding proteins in the primary visual pathway of Pteropus poliocephalus. *J. Comp. Neurol.* 417; 73–87.
35. Jeon, C. J., Spencer, R. F. and Mize, R. R. (1993) Organization and synaptic connections of cholinergic fibers in the cat superior colliculus. *J. Comp. Neurol.* 333; 360–374.
36. Jeon, Y. K., Kim, T. J., Lee, J. Y., Choi, J. S. and Jeon, C. J. (2007) AII amacrine cells in the inner nuclear layer of bat retina: identification by parvalbumin immunoreactivity. *Neuroreport* 18; 1095–1099.
37. Jeong, M. J., Kim, H. G. and Jeon, C. J. (2018) The organization of melanopsin-immunoreactive cells in microbat retina. *PLoS One* 13; e0190435.
38. Jeong, S. J. and Jeon, C. J. (2017) Localization of choline acetyltransferase and tyrosine hydroxylase immunoreactivities in the superior colliculus of the microbat, Rhinolophus ferrumequinum. *Histol. Histopathol.* 32; 609–626.
39. Jones, G. and Teeling, E. C. (2006) The evolution of echolocation in bats. *Trends Ecol. Evol.* 21; 149–156.
40. Kang, J. I., Huppé-Gourgues, F. and Vaucher, E. (2014) Boosting

visual cortex function and plasticity with acetylcholine to enhance visual perception. *Front. Syst. Neurosci.* 8; 172.
41. Kim, H. G., Gu, Y. N., Lee, K. P., Lee, J. G., Kim, C. W., Lee, J. W., Jeong, T. H., Jeong, Y. W. and Jeon, C. J. (2016) Immunocytochemical localization of the calcium-binding proteins calbindin D28K, calretinin and parvalbumin in bat visual cortex. *Histol. Histopathol.* 31; 317–327.
42. Kim, T. J., Jeon, Y. K., Lee, J. Y., Lee, E. S. and Jeon, C. J. (2008) The photoreceptor populations in the retina of the greater horseshoe bat Rhinolophus ferrumequinum. *Mol. Cells* 26; 373–379.
43. Kitt, C. A., Höhmann, C., Coyle, J. T. and Price, D. L. (1994) Cholinergic innervation of mouse forebrain structures. *J. Comp. Neurol.* 341; 117–129.
44. Kruger, J. L., Dell, L. A., Bhagwandin, A., Jillani, N. E., Pettigrew, J. D. and Manger, P. R. (2010) Nuclear organization of cholinergic, putative catecholaminergic and serotonergic systems in the brains of five microchiropteran species. *J. Chem. Neuroanat.* 40; 210–222.
45. Laplante, F., Morin, Y., Quirion, R. and Vaucher, E. (2005) Acetylcholine release is elicited in the visual cortex, but not in the prefrontal cortex, by patterned visual stimulation: A dual *in vivo* microdialysis study with functional correlates in the rat brain. *Neuroscience* 132; 501–510.
46. Lee, J. E., Ahn, C. H., Lee, J. Y., Chung, E. S. and Jeon, C. J. (2004) Nitric oxide synthase and calcium-binding protein-containing neurons in the hamster visual cortex. *Mol. Cells* 18; 30–39.
47. Maseko, B. C. and Manger, P. R. (2007) Distribution and morphology of cholinergic, catecholaminergic and serotonergic neurons in the brain of Schreiber's long-fingered bat, Miniopterus schreibersii. *J. Chem. Neuroanat.* 34; 80–94.
48. Mechawar, N., Cozzari, C. and Descarries, L. (2000) Cholinergic innervation in adult rat cerebral cortex: a quantitative immunocytochemical description. *J. Comp. Neurol.* 428; 305–318.
49. Mesulam, M. M. and Geula, C. (1988) Nucleus basalis (Ch4) and cortical cholinergic innervation in the human brain: observations based on the distribution of acetylcholinesterase and choline acetyltransferase. *J. Comp. Neurol.* 275; 216–240.
50. Mesulam, M. M., Hersh, L. B., Mash, D. C. and Geula, C. (1992) Differential cholinergic innervation within functional subdivisions of the human cerebral cortex: A choline acetyltransferase study. *J. Comp. Neurol.* 318; 316–328.
51. Mesulam, M. M., Mufson, E. J., Wainer, B. H. and Levey, A. I. (1983) Central cholinergic pathways in the rat: An overview based on an alternative nomenclature (Ch1–Ch6). *Neuroscience* 10; 1185–1201.
52. Minces, V. H., Alexander, A. S., Datlow, M., Alfonso, S. I. and Chiba, A. A. (2013) The role of visual cortex acetylcholine in learning to discriminate temporally modulated visual stimuli. *Front. Behav. Neurosci.* 20; 7–16.
53. Moss, C. F. and Sinha, S. R. (2003) Neurobiology of echolocation in bats. *Curr. Opin. Neurobiol.* 13; 751–758.
54. Müller, B., Butz, E., Peichl, L. and Haverkamp, S. (2013) The rod pathway of the microbat retina has bistratified rod bipolar cells and tristratified AII amacrine cells. *J. Neurosci.* 33; 1014–1023.
55. Müller, B., Glösmann, M., Peichl, L., Knop, G. C., Hagemann, C. and Ammermüller, J. (2009) Bat eyes have ultraviolet-sensitive cone photoreceptors. *PLoS One* 4; e6390.
56. Nemoto, C., Hida, T. and Arai, R. (1999) Calretinin and calbindin-D28k in dopaminergic neurons of the rat midbrain: a triple-labeling immunohistochemical study. *Brain Res.* 846; 129–136.
57. Neuweiler, G. (1990) Auditory adaptation for prey capture in echolocating bats. *Physiol. Rev.* 70; 615–641.
58. Nowack, R. M. (1999) Walker's Mammals of the World. 6th ed., The Johns Hopkins University Press, Baltimore.
59. Park, E. B., Gu, Y. N. and Jeon, C. J. (2017) Immunocytochemical localization of cholinergic amacrine cells in the bat retina. *Acta Histochem.* 119; 428–437.
60. Park, H. J., Kong, J. H., Kang, Y. S., Park, S. M., Lim, J. K. and Jeon, C. J. (2002) The distribution and morphology of calbindin D28K- and calretinin-immunoreactive neurons in the visual cortex of mouse. *Mol. Cells* 14; 143–149.
61. Parnavelas, J. G., Kelly, W., Franke, E. and Eckenstein, F. (1986) Cholinergic neurons and fibers in the rat visual cortex. *J. Neurocytol.* 15; 329–336.
62. Pettigrew, J. D., Pettigrew, J. D., Dreher, B., Hopkins, C. S., McCall, M. J. and Brown, M. (1988) Peak density and distribution of ganglion cells in the retinae of microchiropteran bats: implications for visual acuity. *Brain Behav. Evol.* 32; 39–56.
63. Picciotto, M. R., Higley, M. J. and Mineur, Y. S. (2012) Acetylcholine as a neuromodulator: cholinergic signaling shapes nervous system function and behavior. *Neuron* 76; 116–129.
64. Rye, D. B., Wainer, B. H., Mesulam, M. M., Mufson, E. J. and Saper, C. B. (1984) Cortical projections arising from the basal forebrain: a study of cholinergic and noncholinergic components employing combined retrograde tracing and immunohistochemical localization of choline acetyltransferase. *Neuroscience* 13; 627–643.
65. Simmons, N. B. (2000) Bat phylogeny: an evolutionary context for comparative studies. In "Ontogeny, Functional Ecology, and Evolution of Bats", ed. by R. A. Adams and S. C. Pedersen, Cambridge University Press, Cambridge, pp. 9–58.
66. Stichel, C. C. and Singer, W. (1987) Quantitative analysis of the choline acetyltransferase-immunoreactive axonal network in the cat primary visual cortex: I. Adult cats. *J. Comp. Neurol.* 258; 91–98.
67. Suga, N. (1989) Principles of auditory information-processing derived from neuroethology. *J. Exp. Biol.* 146; 277–286.
68. Surlykke, A., Boel Pedersen, S. and Jakobsen, L. (2009) Echolocating bats emit a highly directional sonar sound beam in the field. *Proc. Biol. Sci.* 276; 853–860.
69. Suthers, R. A. and Wallis, N. E. (1970) Optics of the eyes of echolocating bats. *Vision Res.* 10; 1165–1173.
70. Teeling, E. C. (2009) Bats (Chiroptera). In "The Time Tree of Life", ed. by S. B. Hedges and S. Kumar, Oxford University Press, Oxford, pp. 499–503.
71. Wahle, P., Sanides-Buchholtz, C., Eckenstein, F. and Albus, K. (1984) Concurrent visualization of choline acetyltransferase-like immunoreactivity and retrograde transport of neocortically injected markers in basal forebrain neurons of cat and rat. *Neurosci. Lett.* 44; 223–228.
72. Winter, Y., Lopez, J. and Von Helversen, O. (2003) Ultraviolet vision in a bat. *Nature* 425; 612–614.
73. Woolf, N. J. (1991) Cholinergic systems in mammalian brain and spinal cord. *Prog. Neurobiol.* 37; 475–524.
74. Woolf, N. J. and Butcher, L. L. (2011) Cholinergic systems mediate action from movement to higher consciousness. *Behav. Brain Res.* 221; 488–498.
75. Xuan, F., Hu, K., Zhu, T., Racey, P., Wang, X., Zhang, S. and Sun, Y. (2012) Immunohistochemical evidence of cone-based ultraviolet vision in divergent bat species and implication for its evolution. *Comp. Biochem. Physiol. B, Biochem. Mol. Biol.* 161; 398–403.
76. Zhao, H., Xu, D., Zhou, Y., Flanders, J. and Zhang, S. (2009) Evolution of opsin genes reveals a functional role of vision in the echolocating little brown bat (Myotis lucifugus). *Biochem. Syst. Ecol.* 37; 154–161.